Soybean susceptibility to manufactured nanomaterials with evidence for food quality and soil fertility interruption

John H. Priester[a,b,c], Yuan Ge[a,b,c], Randall E. Mielke[a,b,c,d], Allison M. Horst[a,b,c], Shelly Cole Moritz[b], Katherine Espinosa[e], Jeff Gelb[f], Sharon L. Walker[g], Roger M. Nisbet[b,c,h], Youn-Joo An[i], Joshua P. Schimel[b,c,h], Reid G. Palmer[e,j], Jose A. Hernandez-Viezcas[c,k], Lijuan Zhao[c,k], Jorge L. Gardea-Torresdey[c,k], and Patricia A. Holden[a,b,c,1]

[a]Bren School of Environmental Science and Management, [b]Earth Research Institute, and [c]University of California Center for the Environmental Implications of Nanotechnology, University of California, Santa Barbara, CA 93106; [d]Division of Geological and Planetary Sciences, NASA/Jet Propulsion Laboratory, California Institute of Technology, Pasadena, CA 91101; [e]Department of Agronomy, Iowa State University, Ames, IA 50011; [f]Xradia, Pleasanton, CA 94588; [g]Department of Chemical and Environmental Engineering, University of California, Riverside, CA 92521; [h]Department of Ecology, Evolution and Marine Biology, University of California, Santa Barbara, CA 93106; [i]Department of Environmental Science, Konkuk University, Seoul 143–701, Korea; [j]Corn Insects and Crop Genetics Research Unit, Agricultural Research Service, US Department of Agriculture, Ames, IA 50011; and [k]Department of Chemistry, University of Texas at El Paso, El Paso, TX 79968

Based on previously published hydroponic plant, planktonic bacterial, and soil microbial community research, manufactured nanomaterial (MNM) environmental buildup could profoundly alter soil-based food crop quality and yield. However, thus far, no single study has at once examined the full implications, as no studies have involved growing plants to full maturity in MNM-contaminated field soil. We have done so for soybean, a major global commodity crop, using farm soil amended with two high-production metal oxide MNMs (nano-CeO$_2$ and -ZnO). The results provide a clear, but unfortunate, view of what could arise over the long term: (*i*) for nano-ZnO, component metal was taken up and distributed throughout edible plant tissues; (*ii*) for nano-CeO$_2$, plant growth and yield diminished, but also (*iii*) nitrogen fixation—a major ecosystem service of leguminous crops—was shut down at high nano-CeO$_2$ concentration. Juxtaposed against widespread land application of wastewater treatment biosolids to food crops, these findings forewarn of agriculturally associated human and environmental risks from the accelerating use of MNMs.

nanoparticles | nanotechnology | agriculture

As nanotechnology, and the manufactured nanomaterial (MNM) industry specifically, continue rapid expansion (1, 2) and become mainstream, there is concern about buildup in soils and possible MNM entry into the food supply (3). MNMs can enter soil through atmospheric routes (4), e.g., by nano-CeO$_2$ in fuel additives being released with diesel fuel combustion exhaust (5). Another route of entry is from biosolids treated in conventional wastewater treatment plants (WWTPs) (6, 7). Given that half of US biosolids are disposed to land (8), biosolids with MNMs will enter soils (4). The US Environmental Protection Agency mandates pretreatment programs to limit direct industrial metal discharge into publicly owned WWTPs (9) which controls toxic metal buildup in biosolids-amended agricultural soils (10, 11). However, MNMs—although measurable in WWTP systems (12)—are neither monitored nor regulated, have a high affinity for activated sludge bacteria (6), and thus, concentrate in biosolids (12, 13) that are land-applied.

Soybean is a food crop that is vulnerable to such MNM exposure: currently, according to the Food and Agriculture Organization of the United Nations, it is the fifth largest crop in global agricultural production and second in the United States (http://faostat.fao.org/site/339/default.aspx). As of 2009, there were 77.5 million US acres planted with soybean, providing ~40% of world production in this crop and creating a *ca.* $30 billion domestic soybean agricultural economy (14). Soybean provides more edible oil and protein than any other food crop, with most of the seed meal after oil extraction used for livestock feed (14). Soybean agriculture

requires comparatively less nitrogenous fertilizer (e.g., in 2006, 18.5% of soybean acres in the United States were treated with N vs. 96.6% for corn in 2005, per the US Department of Agriculture Agricultural Resource Management Survey Farm Financial and Crop Production Practices; http://www.ers.usda.gov/Data/ARMS/app/default.aspx?survey_abb=CROP) as a result of N$_2$-fixing symbioses (i.e., nodules) arising on soybean roots in soil (15). Fertilizer production is fossil fuel-intensive (16), and N is significantly lost from fertilized fields (17) to increasingly hypoxic coastal zones (18). Thus, replacing synthetic fertilizers with biotic N$_2$ fixation (19) capitalizes on this important ecosystem service (20) provided with cultivating leguminous crops.

Soybean is farmed with fossil fuel-powered equipment that can locally deposit MNMs via exhaust (5), and surrounding fields are routinely amended with WWTP biosolids in the United States (21), suggesting that plants are already exposed to MNMs. In related studies, soybean plants bioaccumulated pharmaceuticals (22) and metals (23) from biosolids-amended soils. Further, hydroponically grown soybean plants bioaccumulated metals or MNMs from nano-ZnO or nano-CeO$_2$ amendments (24), and ZnO and TiO$_2$ MNMs impacted soil microbial community diversity and biomass (25). Together, such reports imply that cultivated soybean exposed to MNMs could be impacted directly or through plant–microbe interactions, including N$_2$ fixing symbioses that are sensitive to some metals (26).

Here, we show that soybean plants, grown fully into bean production, bioaccumulated MNM metals from soil and, in the case of nano-ZnO, translocated significant amounts of metal into leaves and beans. Uptake into roots and root nodules of another MNM, nano-CeO$_2$, eliminated N$_2$ fixation potentials and impaired soybean growth. Thus, in one case (nano-ZnO treatment), the food quality was affected, and in the other (nano-CeO$_2$), soil fertility was compromised. These results indicate broader risks to

the food supply, but also to the environment, as increased synthetic fertilizer use would be required to offset lost N_2 fixation.

Results and Discussion

Nano-CeO$_2$ and Nano-ZnO Differently Affect Aboveground Plant Growth and Yield. Soybean plants were grown through the seed production stage in soil amended with nano-CeO$_2$ (0, 0.1, 0.5, or 1 g·kg^{-1}) or nano-ZnO (0, 0.05, 0.1, or 0.5 g·kg^{-1}). Similar concentrations of these nanoparticles affect hydroponic plants (24, 27) and microorganisms (25, 28), but the effects on soil-cultivated food crop plants are heretofore unknown. Plant growth was monitored by measuring stem length, leaf count, and leaf cover; the latter estimates total leaf area, can indicate plant health, and is affected by water stress (29) and metal exposure (30). Final growth and biomass measurements were made after pod formation and before plant senescence. At harvest, plants were separated into aboveground (stem, leaf, seed pod) and belowground (root, nodule) parts, root nodules were counted, and wet and dry biomasses were measured.

Plant stem length and leaf cover area increased exponentially (Fig. 1 and *SI Appendix*, Fig. S1), and associated first-order growth rate constants (*SI Appendix*, Tables S1 and S2) compared well with typical soybean field (31) and mesocosm (32) studies. The onset of vegetative (*SI Appendix*, Fig. S2) and reproductive (*SI Appendix*, Fig. S3) plant developmental stages were normal. However, plants in the lowest nano-CeO$_2$ treatment grew relatively slowly (*SI Appendix*, Tables S1 and S2).

As a result of substantial variation, some vegetative growth trends were not statistically significant. Still, there were noteworthy observations. For example, the mean leaf count in the high nano-ZnO treatment was significantly lower than the control (10.5 vs. 13.0; $P = 0.02$), but there were no trends with nano-ZnO dose (*SI Appendix*, Fig. S2), and there were no significant effects of nano-ZnO on final leaf cover (*SI Appendix*, Table S2) or maximum stem length (Fig. 1 and *SI Appendix*, Table S1). However, nano-CeO$_2$ at all concentrations reduced the leaf count compared with the control (*SI Appendix*, Fig. S2). Low nano-CeO$_2$ concentrations exerted the most impact on leaf count, and also on total final leaf cover (*SI Appendix*, Fig. S1 and Table S2). Further, plants harvested from the lowest nano-CeO$_2$ treatment were significantly shorter (final stem length; $P = 0.05$) than controls (Fig. 1 and *SI Appendix*, Table S1).

As with the leaf count, there were apparent trends in soybean pod count, subject to substantial variation. For example, within each nanoparticle concentration series, there was a positive dose–response trend, with more pods at high vs. low nanoparticle concentrations (*SI Appendix*, Table S3). This trend was statistically significant when comparing the pod count for the high nano-ZnO

treatment (20 ± 2.9) with the low (13 ± 1.5; $P = 0.05$) and medium (12.8 ± 1.9; $P = 0.05$) nano-ZnO treatments. Across all treatments, soybean pods were similarly sized, averaging 0.84 ± 0.1 cm (width) by 2.84 ± 0.2 cm (length), and the average number of seeds per soybean pod (1.71 ± 0.1) did not vary with treatment.

We observed some variations in water content of MNM-exposed plant tissues, and in the amount of aboveground dry biomass. Stems from the high nano-ZnO treatment, and leaves and pods from all nano-ZnO treatments, were significantly drier (average $P = 0.01$) than control tissues (*SI Appendix*, Table S4). Aboveground dry biomass, however, did not differ significantly when comparing nano-ZnO treatments vs. control (*SI Appendix*, Table S5 and Fig. S4). However, there was a trend with nano-CeO$_2$ treatments such that dry stem and leaf biomass were lower for the low nano-CeO$_2$ treatment, but apparently increased (toward control levels) with medium, then high, nano-CeO$_2$ treatments. The soybean pod dry biomass showed a different trend: all nano-CeO$_2$ treatment levels yielded less biomass compared with the control, with the difference being significant for the high nano-CeO$_2$ treatment ($P = 0.05$; *SI Appendix*, Table S5).

In summary, plant growth was reduced in the low nano-CeO$_2$ treatment, and less soybean pod biomass appeared across all nano-CeO$_2$ treatments (*SI Appendix*, Table S5). In contrast, trends in aboveground biomass, soybean pod biomass, and soybean pod count suggest a stimulatory effect of nano-ZnO (*SI Appendix*, Table S5).

Belowground Biomass and Function Are Affected by Nano-CeO$_2$ and Nano-ZnO. We observed treatment effects belowground on dry biomass and moisture content. Roots from the medium ($P = 0.03$) and high ($P = 0.04$) nano-CeO$_2$ treatments and the medium ($P = 0.01$) and high ($P < 0.005$) nano-ZnO treatments were all significantly drier than the control (*SI Appendix*, Table S4). There was also more dry root biomass for the high nano-ZnO treatment compared with the control ($P = 0.02$; *SI Appendix*, Table S5).

The root nodule counts could indicate impacts on overall nitrogen fixation capacity per plant, but the total number of root nodules per plant (mean = 39 ± 3) were similar across treatments, and were typical (26). However, there was a trend toward drier nodules for the medium and high nano-ZnO treatments (*SI Appendix*, Table S4). Related to these trends, there was significantly more dry nodule biomass for the high nano-ZnO treatment compared with the control ($P = 0.02$; *SI Appendix*, Table S5).

Additionally, the nitrogen fixation potential per nodule was of interest, as variations could indicate MNM effects to the N_2 fixation apparatus. As measured by acetylene reduction to ethylene, the root nodule N_2 fixation potential was similar across the control and nano-ZnO treatments (*SI Appendix*, Table S6). Although N_2 fixation potential appeared to increase in the low nano-CeO$_2$ treatment, the mean was not significantly different from that of control. However, N_2 fixation potentials plummeted, i.e., decreasing by more than 80% relative to the control, in the medium and high nano-CeO$_2$ treatments (*SI Appendix*, Table S6). A similar effect on soybeans was reported with cadmium exposure, whereby high Cd levels dramatically decreased N_2 fixation potentials (26).

In summary, belowground and aboveground biomass was relatively more abundant, but drier, when plants were grown in the presence of nano-ZnO, and the difference vs. controls was significant for high nano-ZnO belowground biomass (*SI Appendix*, Table S4 and Fig. S4). However, for nano-CeO$_2$, there was a more subtle, and functionally important, dose-dependent pattern. Low amounts of nano-CeO$_2$ did not significantly alter N_2 fixation in root nodules (*SI Appendix*, Table S6), but plant growth (above- and belowground) was stunted. With medium and high nano-CeO$_2$, N_2 fixation (*SI Appendix*, Table S6) was inhibited. As exogenous fertilizer was not used, the plants treated with medium and high nano-CeO$_2$ must have compensated for reduced N_2 fixation by acquiring nitrogen as a solute directly from the soil, even though nodules formed (*SI Appendix*, Table S5). Still,
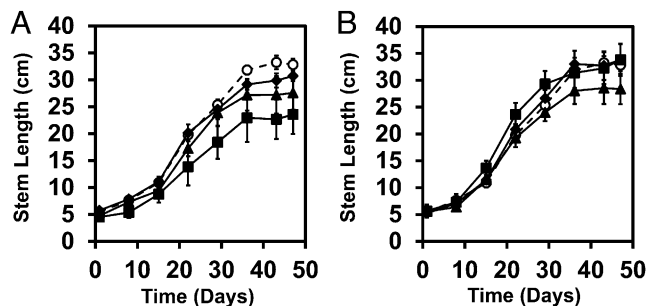
Fig. 1. Soybean stem length vs. time. (*A*) Stem length vs. time for control (○) and nano-CeO$_2$ treatments: low (■), medium (▲) and high (◆). (*B*) Stem length vs. time for control (○) and nano-ZnO treatments: low (■), medium (▲) and high (◆). Error bars represent SEM [$n = 4$ for all groups except low nano-ZnO ($n = 3$)].

Table 1. Concentration of Ce in various plant parts at harvest

| Treatment | Ce concentration, mg Ce·kg⁻¹ dry tissue | | | | |
	Root	Nodule	Stem	Leaf, ×1,000*	Pod
Control	0.296 ± 0.02	0.117 ± 0.02	$0.039 \pm 0.00^{\dagger}$	$0.177 \pm 0.02^{\dagger}$	$0.074 \pm 0.03^{\dagger}$
Low nano-CeO$_2$	0.490 ± 0.07	0.427 ± 0.02	$0.169 \pm 0.05^{\ddagger}$	0.112 ± 0.01	$0.101 \pm 0.02^{\dagger}$
Medium nano-CeO$_2$	$174.46 \pm 28.25^{\dagger}$	$19.83 \pm 5.42^{\dagger}$	$0.206 \pm 0.10^{\dagger,\ddagger}$	$0.247 \pm 0.03^{\dagger,\ddagger}$	0.133 ± 0.07
High nano-CeO$_2$	$210.72 \pm 17.21^{\dagger}$	$11.28 \pm 5.01^{\dagger}$	$0.116 \pm 0.04^{\dagger,\ddagger}$	$0.289 \pm 0.04^{\ddagger}$	$0.090 \pm 0.03^{\dagger}$

$n = 4$ individual plants.
*Multiplied by 1,000; units are µg Ce·kg⁻¹ dry tissue.
†,‡No significant difference within plant part among treatments, i.e., $P > 0.05$ (t test) vs. other entries in the same column with a matching symbol.

there was a cost if the N source was switched from air to soil: pod biomass was diminished, particularly with the high nano-CeO$_2$ treatment (*SI Appendix*, Table S5).

Ce and Zn Accumulate in Different Plant Tissues. Dried plant tissues were assayed for Ce or Zn. Plants grown with nano-CeO$_2$ were also assayed for Zn to assess treatment effects on uptake of background soil Zn. We learned that these MNMs entered and accumulated in plants, and thus are bioavailable in this farm soil. Ce was mobilized from soil and accumulated into the roots with uptake levels similar to those observed in a hydroponic study (24). However, our results show that root nodules also acquire nano-CeO$_2$, a finding only made possible from studying soil-grown plants. Ce concentrations in the roots and nodules from medium and high nano-CeO$_2$ treatments were high, with nearly 400 times more in the roots, and 40 times more in the nodules, than in the low nano-CeO$_2$ treatment (Table 1). However, Ce did not measurably translocate from below- into aboveground biomass (Table 1), and, except for the stems from the high nano-CeO$_2$ treatment, nano-CeO$_2$ did not alter uptake of soil Zn (*SI Appendix*, Table S7).

Like with Ce, we observed substantial amounts of Zn in belowground biomass. For the high nano-ZnO treatment, the roots and root nodules accumulated nearly four times and two times the amount of Zn in the control, respectively (Table 2). Zn concentrations in the control soybean pods were approximately three times higher than typical nutritional levels (34) as a result of background Zn in the study soil (*Methods*). However, unlike Ce, which did not translocate aboveground, Zn substantially moved aboveground from nano-ZnO treated soils: Zn concentrations increased in a dose-dependent fashion in the stem, leaf, and soybean pod tissues, with more than six times more Zn in the stem, four times more in the leaf, and nearly three times more in the soybean pod, when comparing the high nano-ZnO treatment vs. control. The amount of Zn in the leaves was nearly three times greater than that in the stem for the high nano-ZnO treatment, indicating that the leaves were bioaccumulation "hot spots" for Zn (Table 2). Such Zn concentrations in various plant tissues were similar for equivalently dosed soybean (on a Zn

mass basis) grown with Zn salts (33). However, nano-ZnO must have been highly bioavailable in this study soil, as Zn also substantially bioaccumulated in nano-ZnO–treated plants in a previous hydroponic study (24). Very high Zn accumulations could cause long-term impacts to either plant or human health (*SI Appendix*), but the extent and relationship to Zn form (including nano-ZnO) in the plant are unknown.

Metal Accumulations Were Visible by EM. Environmental scanning EM (ESEM; wet mode with a backscatter secondary electron detector), and energy dispersive X-ray spectroscopy (EDS) of embedded fresh plant specimens were used to image and analyze ultrastructural variations and metal accumulation tissue regions. At higher magnification for some tissues, dark-field scanning transmission EM (STEM) with EDS was performed. X-ray microscopy (XRM) was used for one specimen to image metal accumulations in three dimensions across a larger tissue sample.

Because Ce had bioaccumulated in root nodules (Table 1), particularly for the medium and high nano-CeO$_2$ treatments, and because the N$_2$ fixation potential was also severely diminished for these treatments (*SI Appendix*, Table S6), imaging for the nano-CeO$_2$ treatments was prioritized toward root nodules. For the low nano-CeO$_2$ treatment, nodules appeared similar to the control, with apparently similar bacteroid density in plant cells. Electron-dense regions, which would appear bright in ESEM (with backscatter secondary electron detector), were not observed in nodules from the low nano-CeO$_2$ treatment. However, for the high nano-CeO$_2$ treatment, bright regions were observed at low magnification, indicating electron-dense accumulations along the plant cell walls. Bacteroids were relatively absent for the high nano-CeO$_2$ treatment, compared with the control (Fig. 2); this was similar to a report of cadmium effects on root nodule bacteroids (33). The Ce atomic mass percentage, as measured from EDS spectra acquired over select regions (Fig. 2), supported that the nodules from high nano-CeO$_2$ treatments were relatively enriched in Ce compared with the control (*SI Appendix*, Fig. S5). X-ray tomography of a larger nodule tissue specimen from the high nano-CeO$_2$ treatment showed X-ray absorbing regions concentrated along cell walls, appearing as striations (*SI Appendix*, Fig. S6).

Table 2. Concentration of Zn in various plant parts at harvest

| Treatment | Zn concentration, mg Zn·kg⁻¹ dry tissue | | | | |
	Root	Nodule	Stem	Leaf	Pod
Control	31.61 ± 2.12	$19.68 \pm 3.59^{*}$	19.48 ± 1.46	85.59 ± 7.59	$32.04 \pm 2.83^{*}$
Low nano-ZnO	$46.14 \pm 1.44^{*}$	$9.21 \pm 8.03^{*}$	32.94 ± 3.58	125.76 ± 10.14	$38.69 \pm 3.13^{*}$
Medium nano-ZnO	$45.73 \pm 4.10^{*}$	$24.20 \pm 3.61^{*,\dagger}$	46.63 ± 4.27	165.98 ± 15.41	57.46 ± 5.75
High nano-ZnO	123.16 ± 11.67	$34.77 \pm 3.94^{\dagger}$	126.23 ± 8.91	344.07 ± 43.12	81.69 ± 3.19

$n = 4$ individual plants, except for the low nano-ZnO treatment ($n = 3$)
*,†No significant difference within plant part among treatments, i.e., $P > 0.05$ (t test) vs. other entries in the same column with a matching symbol.
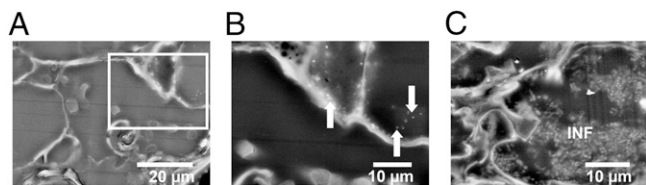
Fig. 2. EM images of soybean root nodules. (*A* and *B*) High nano-CeO₂ treatment. The highlighted region (white rectangle) in *A* is shown in greater detail in *B*. Note the lack of bacteroid cells and the presence of nano-sized particles (arrows). This region was analyzed for Ce content by EDS. (*C*) Control nodule interior shows infection zone (INF) containing bacteroid cells.

EM of nano-ZnO treatments emphasized the seeds and leaves as a result of the high concentration of Zn in these tissues (Table 2). EM images of seeds from the high nano-ZnO treatment revealed bright (i.e., electron-dense) accumulations along cell walls that were not apparent in the control (Fig. 3) and were confirmed by EDS to contain Zn enrichments (*SI Appendix*, Fig. S7). Cross-sections of leaves clearly showed where Zn accumulated in the vascular bundles of high nano-ZnO treatments (Fig. 4), again with EDS confirming the relative enrichment of Zn (*SI Appendix*, Fig. S7). High-resolution dark-field STEM images showed unusual, bright, nano-sized spots in the leaf tissue epidermis and mesophyll tissues, with particularly abundant spots in the epidermis (Fig. 5).

Conclusions

There is great concern, but a dearth of information, regarding potential MNM impacts to agriculture and the food supply (3). Previous soil-grown soybean studies regarded metal salts (33, 35), but studies examining plant–MNM interactions generally used aqueous exposure systems (24, 36–38). There has been contradictory evidence from studying soil microbial communities, i.e., that some MNMs are not bioavailable in soil (39), but also evidence to the contrary for other MNMs (25). Although insight into plant responses to metals and/or MNMs can be gained from hydroponic studies, and MNM impacts on soil microbial communities imply MNM bioavailability, such piecemeal evidence is inadequate to infer how MNMs will impact crops grown in MNM-contaminated soils. Here, soybean plants grown under realistic conditions in MNM-contaminated organic farm soil were impacted in concerning ways. Although nano-ZnO slightly stimulated plant growth, most striking was the degree to which Zn bioaccumulated in all tissues and especially in the leaves. Because the final Zn bioconcentrations were similar to those in a previous study in which soybean was treated with Zn salts (33), Zn that translocated aboveground in the present study may have been substantially dissolved from the nano-ZnO added to the soil. Nano-CeO₂ impacts were different: there was insignificant aboveground translocation, but low nano-CeO₂ exposure stunted plant growth and soybean pod biomass. Further, CeO₂ nanoparticles substantially entered the roots and root nodules, with higher amounts of nano-CeO₂ nearly paralyzing nodule-associated N₂ fixation. In conclusion, this study shows that two high production MNMs are apt to change soybean agriculture, and demonstrates the importance of managing waste streams to control such exposures.

Methods

Soil Source and Characteristics. Organic farm soil was obtained from Carpinteria, CA (N 34° 23′ 40″, W 119° 28′ 40″). The soil was sieved (2 mm), air-dried at room temperature, and stored at 4 °C before use. Sieved soil was characterized (*SI Appendix*, Table S8) by the University of California, Davis, Analytical Laboratory (http://anlab.ucdavis.edu/) for texture, pH, saturation, cation exchange capacity, soluble salts, organic matter, total nutrients (C, Cu, Fe, Mn, N, Zn), extractable nutrients (B, Ca, Cl, Cu, Fe, Mg, Mn, Na, P, Zn, HCO₃, CO₃, NH₄, NO₃), and exchangeable nutrients (Ca, K, Mg, Na).

Nanoparticles and Addition to Soil. Nano-ZnO and nano-CeO₂ (Meliorum Technologies), described by the manufacturer as having mean diameters of ∼10 nm and ∼8 nm, respectively, were added to the soil ∼24 h before planting. Nanoparticles initially were added as a powder to soil in concentrations (dry mass/dry mass basis) of 5, 10, and 50 g·kg⁻¹ for ZnO, and 10, 50, and 100 g·kg⁻¹ for CeO₂. The nanoparticles were mixed mechanically (5 min with separate handheld kitchen mixers) into the soil. The nanoparticles were diluted twice by the addition of unspiked soil into each mixture. After each dilution, the soil/nanoparticle mixtures were mixed as described earlier. The first dilution resulted in concentrations of 0.5, 1, and 5 g·kg⁻¹ for ZnO, and 1, 5, and 10 g·kg⁻¹ for CeO₂. The second dilution resulted in the working concentrations of 0.05, 0.1, and 0.5 g·kg⁻¹ for ZnO, and 0.1, 0.5, and 1.0 g·kg⁻¹ for CeO₂. The soil/nanoparticle mixtures were stored at 4 °C before planting.

Bacterial Strain, Test Plant, and Application. *Bradyrhizobium japonicum* strain USDA 110 (US Department of Agriculture) was reconstituted from a lyophilized culture by using modified arabinose gluconate medium, pH 6.6 (component concentrations g·L⁻¹, Hepes, 1.3; Mes, 1.1; yeast extract, 1.0; arabinose, 1.0; gluconic acid, 1.0; KH₂PO₄, 0.22; Na₂SO₄, 0.25; NH₄Cl, 0.32; FeCl₃, 0.0067; CaCl₂, 0.015; and MgSO₄, 0.18). The culture was incubated for 5 d at 30 °C (dark, shaking at 200 rpm). Following incubation, the culture was centrifuged (10,000 × g, 10 min) and the supernatant discarded. The cell pellet was resuspended in 1 M MgSO₄ to an optical density of 1.0 (λ value, 600 nm). Dwarf soybean seeds (variety Early Hakucho, product no. 5555) were purchased from Park Seed Company. All seeds were selected from the same lot (no. AD40). Soybean seeds were soaked in the resuspended cells for 10 min before being inserted into 4-cm-diameter peat-filled seed starting pellets. Following seed planting, 100 μL of the resuspended *B. japonicum* culture was deposited into the peat pellet holes. The holes were covered with a thin layer of soil, and the pellets were placed in the greenhouse for seedling growth. The pellets were contained in a shallow PVC tray and were watered daily to ensure continuous moisture. Cotyledons emerged from the seed peat pellets after 4 to 7 d.

Planting. Four-liter polyethylene/polypropylene blend garden pots were lined at the base (inner) with polyethylene mesh (Easy Gardener). To aid in water drainage and prevent root rot, ∼400 g of washed gravel (1.25–2.5 cm) was placed above the polypropylene mesh. The soil was contained within polyethylene bags placed within the garden pots and above the gravel. The bags enclosed the entire root system and allowed for easier removal from the pots at harvest time. Each bag was perforated with 5 mm holes (n = 20) to allow for drainage. Eight pots, each containing 2.4 kg of soil, were prepared for each of the seven treatments (nanoparticle-free control, nano-CeO₂ at 0.1, 0.5, and 1.0 g·kg⁻¹, and nano-ZnO at 0.05, 0.1, and 0.5 g·kg⁻¹). Four of the eight pots from each treatment received transplanted seedlings, whereas the remaining pots served as unplanted controls. At the center of each pot receiving a seedling, at the soil surface, a 3.8-cm-diameter, 5-cm-deep hole was drilled for the placement of transplanted seedlings.

Seedlings (including the peat pellets) were transplanted to the pots once the true leaves emerged [stage VC (40); 18 d after planting; *SI Appendix*, Fig. S8]. Before transplanting, the seedlings were ranked according to size into four classes. Each treatment received one seedling from each size class. We began taking measurements three days after seedlings had been transplanted (i.e., time 0).

Soil Sensing of Water Content, Temperature, and Conductivity. Model 5TE sensors (Decagon) were inserted to a depth of 13 cm into the soil of 10 pots: control (with and without plant), 0.1 g·kg⁻¹ nano-CeO₂ (with and without
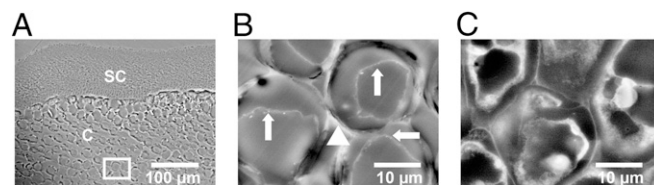
Fig. 3. EM images of soybean seeds. (*A* and *B*) High nano-ZnO treatment. The seed coat (SC) and cotyledon tissue (marked with "C") are visible. *B* is a magnification from a region of *A* (white rectangle). Regions of high electron density (triangle, *B*) were enriched with Zn according to EDS. Nano-sized accumulations within cells (arrows) were visible. (*C*) Control soybean: the bright electron-dense regions between cells are not apparent as in the high nano-ZnO treatment. Nano-sized accumulations are also not visible in the control.
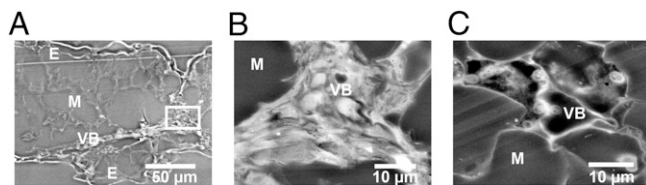
Fig. 4. EM images of soybean leaf cross-sections. (*A* and *B*) High nano-ZnO treatment. The epidermis (marked with "E"), mesophyll ("M"), and vascular bundles (VB) are visible. A vascular bundle cross-section in *A* is highlighted (white rectangle) and magnified to higher resolution in *B*. The nano-ZnO–exposed vascular bundles were highly electron-dense, as indicated by the intense brightness, and showed an elevated Zn signal in EDS compared with controls. (*C*) Control leaf section show a vascular bundle and mesophyll. The control vascular bundles exhibited less electron density (i.e., less brightness), and were not enriched with Zn according to EDS.

plant), 1.0 g·kg^{-1} nano-CeO$_2$ (with and without plant), 0.05 g·kg^{-1} nano-ZnO (with and without plant), and 0.5 g·kg^{-1} nano-ZnO with and without plant). Water content, conductivity, and temperature were measured immediately before and after each watering by using a ProCheck data recorder (Decagon; *SI Appendix*, Figs. S9–S11).

Greenhouse Conditions. The experiment was conducted in a climate-controlled greenhouse under full sunlight. The nominal maximum temperature in the greenhouse was set at 27 °C. Temperatures during a typical 60-h span (days 7–9) fluctuated between a maximum of 31 °C and a minimum of 12 °C.

Watering. The pots (with and without plants) were watered with tap water, on average, once every 72 h to achieve an average soil water content of 0.15 m^3·m^{-3} (*SI Appendix*, Fig. S9). Initially, the planted and unplanted pots were watered with equal volumes (100 mL). As a result of increased water loss from transpiration and growth, the planted pots received averages of 200 mL per watering from days 9 to 21, 250 mL per watering from days 21 to 27, and 300 mL per watering from day 27 until the completion of the experiment. The unplanted pots received an average of 100 mL per watering for the duration of the experiment.

At each watering, a subsample of H$_2$O was removed and measured for Zn and Ce concentrations by inductively coupled plasma (ICP) atomic emission spectroscopy. Ce was not present in measurable concentrations in the irrigation water. Zn was present in concentrations ranging from 0 to 0.17 mg·L^{-1}, and accounted for a cumulative addition of <0.1 mg per pot.

Plant Growth Metrics. At weekly intervals, the number of leaves, flowers, and pods were counted and stem length (as a proxy for plant height) measured. Additionally, the reproductive and vegetative developmental stages of each plant were recorded. To estimate total leaf area, we measured leaf cover from aerial images taken directly above the plant. Leaf cover (calculated by using Adobe Photoshop software) was defined as the percentage of soil covered by the leaves (*SI Appendix*, Fig. S12). This does not give an absolute value of total leaf area (because of leaf overlap), but provides a dynamic estimate that can be used for comparison across treatments.

Harvesting Description. The plants were harvested after ~48 d of growth [developmental stage R5 (40); *SI Appendix*, Fig. S8]. Aboveground plant tissue was removed from the root system with a razorblade, and mass was immediately measured. The plants were then divided according to tissue type—stem, leaves, and pods—and weighed separately. Leaves and pods were photographed for size analysis and leaf cover measurements, respectively. Subsamples of each tissue type were removed and refrigerated (4 °C) for examination with EM. The remaining tissues were oven-dried (70 °C for 72 h) separately in paper bags before ICP optical emission spectroscopy (OES) analysis. Masses were recorded before and after drying to determine dry mass and water content.

The root system of each plant was removed by first carefully breaking apart the soil with a metal Scoopula, followed by a rinse (1 min, three times) in deionized (DI) H$_2$O. The root system was allowed to air dry (~15 min) before weighing for wet mass. Nodules were removed from the roots by using forceps, massed, and allocated for N$_2$ fixation potential, ICP-OES analysis, and EM. The nodules for N$_2$ fixation potential were used immediately. Nodules for EM were refrigerated (4 °C) until use. Nodules for ICP-OES analysis were massed, oven-dried (70 °C for 72 h), and massed a second time to determine

water content. Root tissue for EM was refrigerated (4 °C) until use. Root tissue for ICP-OES analysis was dried and massed as described earlier. Soil from planted and unplanted pots was stored (4 °C and −80 °C) for future analysis.

Acetylene Reduction. Acetylene (C$_2$H$_2$) can be reduced to ethylene (C$_2$H$_4$) by nitrogenase, the enzyme responsible for catalyzing N$_2$ fixation by bacteria in root nodules. C$_2$H$_2$ conversion to C$_2$H$_4$, quantified by gas chromatography, provides evidence of nodule activity and N$_2$ fixation (41). To quantify effects of nanoparticle exposure on nitrogenase activity in soybean root nodules, C$_2$H$_2$ reduction to C$_2$H$_4$ by collected nodules was measured as described previously (41) with several adjustments. Briefly, C$_2$H$_2$ was generated by combining several grams of solid calcium carbide (CaC$_2$) with deionized water in a 1-L plastic bottle. The gas was immediately collected in a sterile bladder with a septum. Root nodules collected from individual plants were gently washed and placed in sterile 60-mL plastic syringes. The syringes were filled with 54 mL of air, followed by 6 mL of C$_2$H$_2$, to yield 60 mL of a 10% C$_2$H$_2$ mixture. At 0, 15, 30, 45, and 60 min after C$_2$H$_2$ addition, 10 mL of gas from the syringe was injected manually into the gas chromatograph (SRI 8610; SRI Instruments) equipped with a silica gel column. The oven temperature was held constant at 145 °C, with a carrier flow rate of 20 mL·min^{-1} Two distinct peaks were observed, with C$_2$H$_4$ having a shorter retention time (~1.09 min) compared with C$_2$H$_2$ (~1.73 min). Peak areas were estimated by using an integration tool (PeakSimple 2.83; SRI Instruments), and were converted into C$_2$H$_2$ and C$_2$H$_4$ concentrations by using data from standard curves. Calculations accounted for the decrease in total volume space over the course of sampling (i.e., the 10-mL reduction in volume at each reading). C$_2$H$_4$ production rates (in mol/min) were normalized to the total dry mass of nodules in each sample (in mol/min/g).

ICP-OES and ICP-MS Analyses. Soil and tissue samples were analyzed for MNM metal content by ICP. Before ICP analysis, samples were digested by using a microwave acceleration reaction system (CEMCorp). Plant tissue samples treated with nano-ZnO were digested by using Environmental Protection Agency method 3051. Soil samples were digested with a mixture of concentrated plasma-pure HNO$_3$ and HCl (1:3; i.e., aqua regia). The nano-CeO$_2$ treated samples were digested with concentrated plasma-pure HNO$_3$ and H$_2$O$_2$ [30% (vol/vol); 1:4] as described previously (42) with slight modifications.

Ten blanks were analyzed to calculate the detection limit for Zn and Ce. Standard reference materials from National Institute of Standards and Technology 1547, 1570a, and 2709a were used to validate the digestion and analytical method obtaining recoveries between 90% and 99%. For quality control of the ICP readings, every 10 samples, the blank and a spiked sample containing Ce and Zn at 10 mg·L^{-1} were read. The average readings for Ce and Zn in the spiked samples were 10.1 ± 0.30 mg·L^{-1} and 9.9 ± 0.20, respectively.

The total Ce and Zn concentrations in the tissues and soil were determined using ICP-OES (Optima 4300 DV; Perkin-Elmer) and ICP-MS (ELAN DRC II; Perkin-Elmer). Zn-treated samples were analyzed with ICP-OES, whereas Ce-treated and control samples were analyzed with ICP-OES and ICP-MS. ICP-MS allowed for the detection of trace amounts of Ce in the plant tissue. The ICP-OES parameters used were as follows: nebulizer flow, 0.80 L·min^{-1}; power, 1,450 W; peristaltic pump rate, 1.5 mL·min^{-1}; flush time, 15 s; delay time, 20 s; read time, 10 s; and wash time, 60 s. Every sample was read in triplicate. The ICP-MS parameters used were as follows: plasma radiofrequency power, 1,400 W; plasma gas flow (Ar), 18 l min^{-1}; scanning mode peak hopping; nebulizer flow, 0.95 l min^{-1}; dwell time, 35 ms; sweeps, 30; and replicates, 3.

EM and EDS. To determine metal localization in plant tissues, samples were visualized by EM; elemental analysis during EM was by EDS. Soybean plant tissues were fixed with 2% glutaraldehyde for 24 h before embedding in
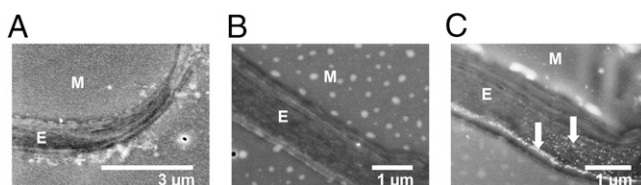
Fig. 5. High-resolution EM images of soybean leaf tissue. All panels show the epidermis (marked with "E") and mesophyll ("M"). No electron-dense accumulations are visible in leaf from control (*A*) or high nano-CeO$_2$ treatment (*B*). In the high nano-ZnO treatment (*C*), numerous nano-sized accumulations (arrows) are visible, and are concentrated at the outer region of the epidermis.

Eponate 12 resin (100% vol/vol; cured at 60 °C for 24 h) and sectioning (5 μm thickness) for analysis by ESEM using a backscatter secondary electron detector and high-resolution STEM (60 nm thickness). Thin sections for ESEM were deposited on carbon tape on a 100% silicon substrate. For STEM, thin sections were placed on a Formvar-coated 200 mesh copper grid. An XL30 ESEM FEG microscope (FEI) was used for ESEM and STEM. ESEM was performed with a 20-kV accelerating voltage, 4-Torr chamber pressure, and 10.2-mm working distance under environmental (i.e., wet) mode. For STEM, the microscope was operated with an attached STEM detector at an accelerating voltage of 30 kV with a 6.8-mm working distance under high vacuum mode. EDS was performed on selected areas of 25 μm^2 (for ESEM) and 100 nm^2 (for STEM) by using an X-ray spectrometer (EDAX) with Genesis analytical software. The spectra were analyzed to obtain mass percentages for Zn and Ce when including (Na, Mg, Al, Si, P, S Cl, K, Ca, CeL, Fe, Zn) in the analytical elemental parameter.

XRM. XRM allowed for the visualization of MNM metal distribution over large specimen regions, relative to EM. Dried root specimens were mounted to a thin wire and imaged in 3D by using laboratory XRM. For these experiments, the Xradia UltraXRM-L200 microscope (Xradia) was used, operating at 8 keV and configured for 150-nm resolution with a 65-μm field of view. The Zernike phase-contrast imaging mode was used to enhance the contrast of the root matrix interfaces and internal materials, including the CeO_2 nanoparticles (43). Transmission X-ray micrographs were collected across a 180° rotation range in 0.2° steps, with a 4-min integration time per view. The resulting tomography series was reconstructed by using the XMReconstructor software package, which produced a stack of tomograms corresponding to virtual slices inside the specimen. These tomograms were finally loaded into the XM3DViewer software for 3D visualization in planar and volumetric formats.

Statistical Analyses. Statistical analyses of sample replicates were performed by using Microsoft Excel 2010 software. Means were compared using Student's t test, assuming a two-tailed distribution and two-sample unequal variance. Tested sample sizes were $n = 4$ except for the low nano-ZnO treatment ($n = 3$). Plant leaf cover and stem length elongation rates were calculated as the slope of a regression line from the linear region of the plot of the natural logarithm of each measured parameter vs. time. When applicable, SEs were calculated and propagated according to standard methods (44).

1. Hullmann A (2007) Measuring and assessing the development of nanotechnology. *Scientometrics* 70:739–758.
2. Roco MC (2011) The long view of nanotechnology development: The National Nanotechnology Initiative at 10 years. *J Nanopart Res* 13:427–445.
3. Rico CM, Majumdar S, Duarte-Gardea M, Peralta-Videa JR, Gardea-Torresdey JL (2011) Interaction of nanoparticles with edible plants and their possible implications in the food chain. *J Agric Food Chem* 59:3485–3498.
4. Nowack B, et al. (2012) Potential scenarios for nanomaterial release and subsequent alteration in the environment. *Environ Toxicol Chem* 31:50–59.
5. Cassee FR, et al. (2011) Exposure, health and ecological effects review of engineered nanoscale cerium and cerium oxide associated with its use as a fuel additive. *Crit Rev Toxicol* 41:213–229.
6. Kiser MA, Ryu H, Jang HY, Hristovski K, Westerhoff P (2010) Biosorption of nanoparticles to heterotrophic wastewater biomass. *Water Res* 44:4105–4114.
7. Brar SK, Verma M, Tyagi RD, Surampalli RY (2010) Engineered nanoparticles in wastewater and wastewater sludge—evidence and impacts. *Waste Manag* 30:504–520.
8. US Environmental Protection Agency (2012) Water: Sewage Sludge (Biosolids). Frequently Asked Questions. Available at http://water.epa.gov/polwaste/wastewater/treatment/biosolids/genqa.cfm. Accessed August 3, 2012.
9. US Environmental Protection Agency (2011) *Introduction to the National Pretreatment Program* (Office of Wastewater Management, Environmental Protection Agency, Washington, DC).
10. McBride MB (2003) Toxic metals in sewage sludge-amended soils: Has promotion of beneficial use discounted the risks? *Adv Environ Res* 8:5–19.
11. Holt LM, Laursen AE, McCarthy LH, Bostan IV, Spongberg AL (2010) Effects of land application of municipal biosolids on nitrogen-fixing bacteria in agricultural soil. *Biol Fertil Soils* 46:407–413.
12. Kiser MA, et al. (2009) Titanium nanomaterial removal and release from wastewater treatment plants. *Environ Sci Technol* 43:6757–6763.
13. Wang YF, Westerhoff P, Hristovski KD (2012) Fate and biological effects of silver, titanium dioxide, and C60 (fullerene) nanomaterials during simulated wastewater treatment processes. *J Hazard Mater* 201-202:16–22.
14. Economic Research Service, United States Department of Agriculture (2012) Briefing room: Soybeans and oil crops. Background. Available at http://www.ers.usda.gov/topics/crops/soybeans-oil-crops.aspx. Accessed August 3, 2012.
15. Salvagiotti F, et al. (2008) Nitrogen uptake, fixation and response to fertilizer N in soybeans: A review. *Field Crops Res* 108:1–13.
16. Galloway JN, et al. (2008) Transformation of the nitrogen cycle: Recent trends, questions, and potential solutions. *Science* 320:889–892.
17. Schlesinger WH (2009) On the fate of anthropogenic nitrogen. *Proc Natl Acad Sci USA* 106:203–208.
18. Vitousek PM, et al. (1997) Human alteration of the global nitrogen cycle: Sources and consequences. *Ecol Appl* 7:737–750.
19. Herridge DF, Peoples MB, Boddey RM (2008) Global inputs of biological nitrogen fixation in agricultural systems. *Plant Soil* 311:1–18.
20. Costanza R, et al. (1997) The value of the world's ecosystem services and natural capital. *Nature* 387:253–260.
21. Currie VC, Angle JS, Hill RL (2003) Biosolids application to soybeans and effects on input and output of nitrogen. *Agric Ecosyst Environ* 97:345–351.
22. Wu CX, Spongberg AL, Witter JD, Fang M, Czajkowski KP (2010) Uptake of pharmaceutical and personal care products by soybean plants from soils applied with biosolids and irrigated with contaminated water. *Environ Sci Technol* 44:6157–6161.
23. Berti WR, Jacobs LW (1996) Chemistry and phytotoxicity of soil trace elements from repeated sewage sludge applications. *J Environ Qual* 25:1025–1032.
24. López-Moreno ML, et al. (2010) Evidence of the differential biotransformation and genotoxicity of ZnO and CeO_2 nanoparticles on soybean (*Glycine max*) plants. *Environ Sci Technol* 44:7315–7320.
25. Ge Y, Schimel JP, Holden PA (2011) Evidence for negative effects of TiO_2 and ZnO nanoparticles on soil bacterial communities. *Environ Sci Technol* 45:1659–1664.
26. Chen YX, et al. (2003) Effect of cadmium on nodulation and N_2-fixation of soybean in contaminated soils. *Chemosphere* 50:781–787.
27. López-Moreno ML, de la Rosa G, Hernández-Viezcas JA, Peralta-Videa JR, Gardea-Torresdey JL (2010) X-ray absorption spectroscopy (XAS) corroboration of the uptake and storage of CeO_2 nanoparticles and assessment of their differential toxicity in four edible plant species. *J Agric Food Chem* 58:3689–3693.
28. Pelletier DA, et al. (2010) Effects of engineered cerium oxide nanoparticles on bacterial growth and viability. *Appl Environ Microbiol* 76:7981–7989.
29. Gutierrez-Boem FH, Thomas GW (2001) Leaf area development in soybean as affected by phosphorus nutrition and water deficit. *J Plant Nutr* 24:1711–1729.
30. Weryszko-Chmielewska E, Chwil M (2005) Lead-induced histological and ultrastructural changes in the leaves of soybean (*Glycine max* (L.) Merr.). *Soil Sci Plant Nutr* 51:203–212.
31. Taylor HM, Mason WK, Bennie ATP, Rowse HR (1982) Responses of soybeans to 2 row spacings and 2 soil-water levels. 1. An analysis of biomass accumulation, canopy development, solar-radiation interception and components of seed yield. *Field Crops Res* 5:1–14.
32. Killion DD, Constantin MJ, Siemer EG (1971) Acute gamma-irradiation of soybean plant: Effects of exposure, exposure rate and developmental stage on growth and yield. *Radiat Bot* 11:225–232.
33. Shute T, Macfie SM (2006) Cadmium and zinc accumulation in soybean: A threat to food safety? *Sci Total Environ* 371:63–73.
34. Messina MJ (1999) Legumes and soybeans: Overview of their nutritional profiles and health effects. *Am J Clin Nutr* 70(3 suppl):439S–450S.
35. Li PJ, et al. (2011) Effects of sulfur dioxide pollution on the translocation and accumulation of heavy metals in soybean grain. *Environ Sci Pollut Res Int* 18:1090–1097.
36. Lin DH, Xing BS (2008) Root uptake and phytotoxicity of ZnO nanoparticles. *Environ Sci Technol* 42:5580–5585.
37. Kurepa J, et al. (2010) Uptake and distribution of ultrasmall anatase TiO_2 Alizarin red S nanoconjugates in *Arabidopsis thaliana*. *Nano Lett* 10:2296–2302.
38. Cifuentes Z, et al. (2010) Absorption and translocation to the aerial part of magnetic carbon-coated nanoparticles through the root of different crop plants. *J Nanobiotechnology* 8:1–8.
39. Tong Z, Bischoff M, Nies L, Applegate B, Turco RF (2007) Impact of fullerene (C60) on a soil microbial community. *Environ Sci Technol* 41:2985–2991.
40. Fehr WR, Caviness CE, Burmood DT, Pennington JS (1971) Stage of development descriptions for soybeans *Glycine max* (L.) Merrill. *Crop Sci* 11:929–931.
41. Weaver RW, Danso SKA (1994) Dinitrogen Fixation. *Methods of Soil Analysis Part 2-Microbiological and Biochemical Properties*, eds Weaver RW, Angle JS, Bottomley PS (Soil Science Society of America, Madison, WI), pp 1019–1045.
42. Packer AP, et al. (2007) Validation of an inductively coupled plasma mass spectrometry (ICP-MS) method for the determination of cerium, strontium, and titanium in ceramic materials used in radiological dispersal devices (RDDs). *Anal Chim Acta* 588:166–172.
43. Tkachuk A, et al. (2007) X-ray computed tomography in Zernike phase contrast mode at 8 keV with 50-nm resolution using Cu rotating anode X-ray source. *Z Kristallogr* 222:650–655.
44. Taylor JR (1997) *An Introduction to Error Analysis: The Study of Uncertainties in Physical Measurements* (University Science Books, Sausalito, CA), 2nd Ed.